

According to Fig. 10 the feed water flow rate is limited to the minimum value after about 10 minutes.

Fig. 12 shows the temperature curve at the outlet of super-heater 2, where the material 10CrMo910 is connected to Incoloy 800. The curve of the values measured in point T 130 located on a tube of the 14. helicoil, is in good agreement with the calculated values. The curve indicating the measuring values T 126, however, does not show any new rise of temperatures.

The measuring point T 126 is situated on a tube of the innermost helicoil on which the adjustment of the throttle valves had not yet been performed at that time. In the measuring point 127 some periodic temperature fluctuations were observed.

Fig. 13 shows the steam temperature curves at the outlet of the high-pressure bundle and Fig. 14 shows the steam temperature curve at the main steam header outlet which due to its wall thickness of 36 mm is the component of the steam generator which is exposed to the maximum loads resulting from temperature transients. In addition, a temperature curve is plotted in this figure which had been taken as a basis of the stress analysis.

The fatigue life fraction used up by the decay heat removal procedures up to the 2nd of September, 1986 was calculated for two components whose main loads result from temperature transients.

The fatigue life fraction of the HP-thermosleeves by which the main steam system line is connected to the support plate of the central tube is 1 %. The fatigue life fraction of the main steam header is 0.51 %, while the ratcheting life fraction regarding peak strain is 6.2 %.

## MECHANICAL DESIGN OF THE HOT STEAM HEADERS OF THE THTR-300 STEAM GENERATORS

U. BLUMER  
Sulzer Brothers Ltd,  
Winterthur, Switzerland

M. STUMPF  
EVT Stuttgart,  
Stuttgart, Federal Republic of Germany

### Abstract

#### General

The high pressure steam headers of the THTR steam generators have been subject to special attention during the design phase due to the following reasons:

- These components are the pressure retaining parts with the heaviest wall thickness in the region of the steam generators.
- They therefore are sensitive to thermal transient conditions.
- They are operated in the elevated temperature regime, where creep effects cannot be neglected.
- There is almost no service experience from fossil steam generators with this type of material (Alloy 800).

Safety consideration therefore have been rather extensive and have focussed on two main areas which will be treated in this paper:

1. Analytical investigations on the cyclic material behaviour under all specified operating conditions, taking into account the non-elastic response of the material.
2. Limitation of the consequences of a header rupture by installation of heavy whip restraints.

#### Elastic-plastic-creep analyses

The analyses were performed in different stages and are explained in the corresponding order:

- Evaluation of the critical location on the header and establishment of a simplified model of a nozzle region for further analysis.
- Preliminary thermal analyses of all specified transient conditions on simplified procedures, in order to establish a

severity ranking of the conditions. Establishment of representative loading blocks.

- Evaluation of the material properties for thermal and structural, especially non-elastic behaviour.
- Detailed thermal analyses.
- Detailed structural analyses of the non-elastic cyclic response.
- Extrapolation for all cycles and assessment of the results by design codes.
- Discussion of the results.

#### Header whip restraint design

In addition to the above analysis efforts, heavy whip restraints were provided to assure limitation of the effects of a header failure. This paper shows the measures that were taken to restrain the movement in case of longitudinal and transverse breaks: The anti-whip designs are presented as well as the analyses that were performed to show their structural adequacy.

#### Introduction

Fig. 1 shows the arrangement of the steam system in the THTR 300 MW plant. The 6 steam generators receive and send the water/steam of high and medium pressure through piping that is connected with four headers each, located in the upper concrete ring wall.

The high pressure steam headers of the steam generators have been subject to special attention during the design phase due to the following reasons:

- These components are the pressure retaining parts with the heaviest wall thickness in the region of the steam generators.
- They therefore are sensitive to thermal transient conditions.
- They are operated in the elevated temperature regime, where creep effects cannot be neglected.
- There is almost no service experience from fossil steam generators with this type of material (Alloy 800).

Safety considerations therefore have been rather extensive and have focussed on two main areas which will be treated in this paper:

1. Analytical investigations on the cyclic material behaviour under all specified operating conditions, taking into account the nonelastic response of the material.
2. Limitation of the consequences of a header rupture by installation of heavy whip restraints.

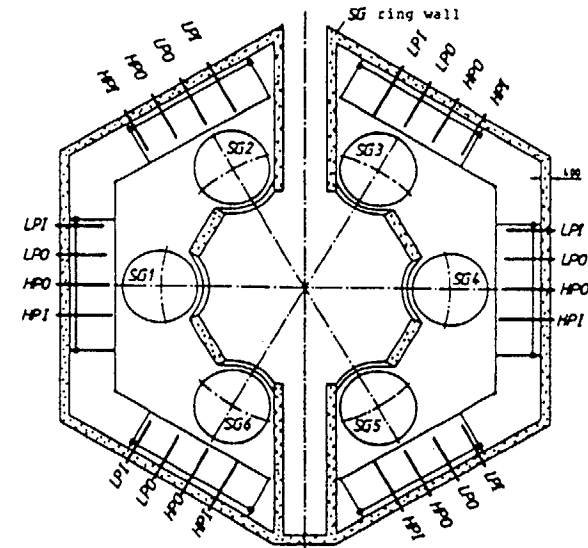


Fig.1 Steam System of THTR 300 MW

1. Investigation on thermal cyclic behaviour
- 1.1 The geometry of the headers

The geometry of the headers is given in fig. 2. It shows the basic form without its fixation on the building structures. The header collects the steam from 40 tubes in four rows. The right end has an end plate with an inspection tube attached, whereas the steam leaves by the left end past a temperature measuring nozzle and a drainage nozzle. The whole header is guided by the right end and fixed by a thermal sleeve at the left end. Preliminary studies were done to determine the location that is critical for thermal loading by steam transients. From the three locations: transition to thermal sleeve, transition to right end plate and steam inlet nozzle, the latter was found to be most sensitive. It was therefore decided to analyse this region in detail.

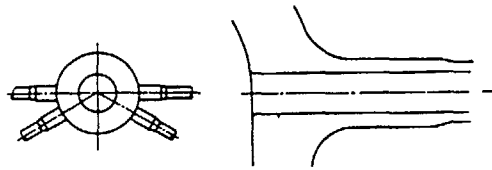
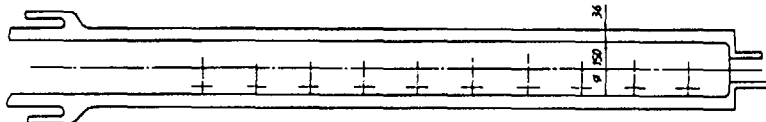


Fig. 2  
The geometry  
of the HP  
outlet header

After preliminary analyses it was found that the justification of the design was not possible on the basis of purely elastic analyses. However it is known that the elastic stress criteria can be overly conservative and it was determined that finite element calculations including plastic and creep response of the material were required. Fig. 3 shows the finite element mesh that was chosen to analyse the region of the nozzle. The basic header cylinder was replaced by a sphere geometry with the same wall thickness and a radius that produces the same pressure hoop stresses.

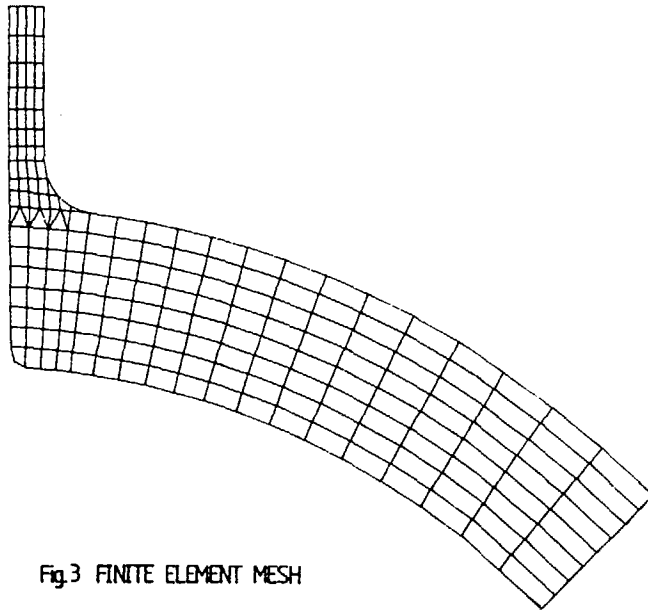


Fig. 3 FINITE ELEMENT MESH

## 1.2 The thermal loadings

The thermal conditions of the live steam system of the THTR have been specified with about 30 different transient operational conditions that have to be considered. For an elastic-plastic-creep analysis it would have been a practical impossibility to analyze all these transient conditions in a manner following an assumed time history of the events with their respective cycle numbers. It was therefore necessary to use a simple filtering approach to discern the relevant transient conditions from the less important ones. This was done by analyzing all transient conditions in one-dimensional thermal calculations, using an undisturbed header cylinder with mass flows at its left end. The resulting transient temperature gradients in this wall create bending moments that can be characterized by the respective equivalent linear temperature difference across the wall thickness. This procedure allows the determination of a severity ranking of all operational conditions. Fig. 4 shows this ranking graphically. The abscissa shows the cumulative cycle numbers of the different conditions. The ordinate represents the linearized temperature difference across the wall,  $\Delta T_1$ . It can be seen that the function follows approximately a

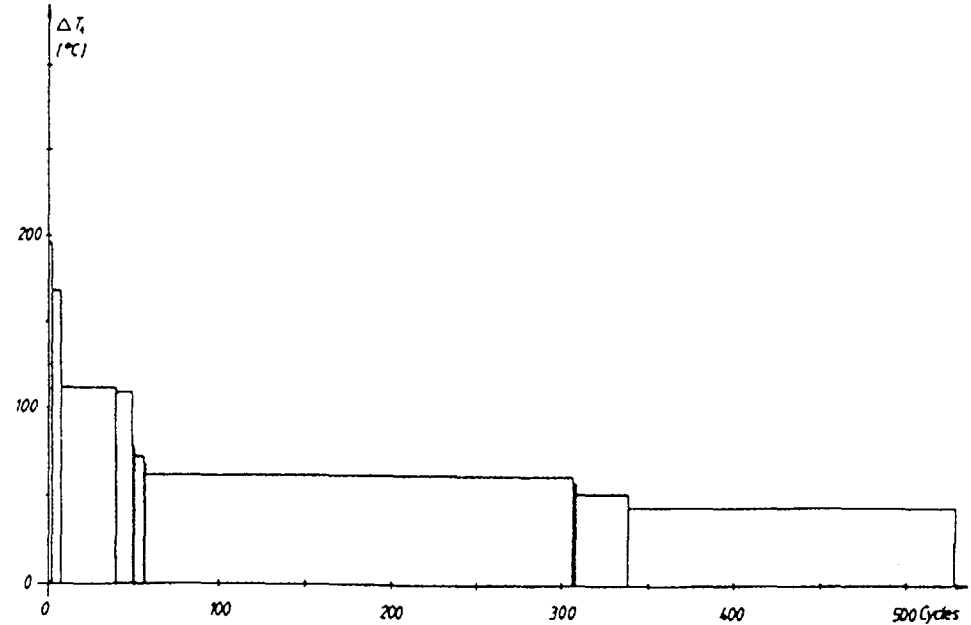


Fig. 4 Temperature gradients of the transients  
as a Function of cumulative Cycle number

hyperbolic function, i.e. there are relatively few very severe transient conditions and gradually more frequent conditions with lower temperature differences. This graph was used to lump all conditions into three blocks with  $DT_1$  values and cycle numbers that cover the actual function conservatively, the first block having a  $DT_1$  of almost 200 deg C and a cumulative cycle number of 7.

### 1.3 The material behaviour

The material used for the headers is alloy 800, grade 1, which was supposed to have advantages over the commonly used alloy 800 H, grade 2, at the long term operating temperatures of around 560 deg C. At this temperature creep effects are not dominant and therefore the solution annealed grade 2 form would not be any better. The specified yield strength of the header material is higher than for the solution annealed grade.

For the inelastic analysis it was decided to use plastic behaviour data from uniaxial specimen tests with cyclic strain loading. Fig. 5 shows the results of such a test with

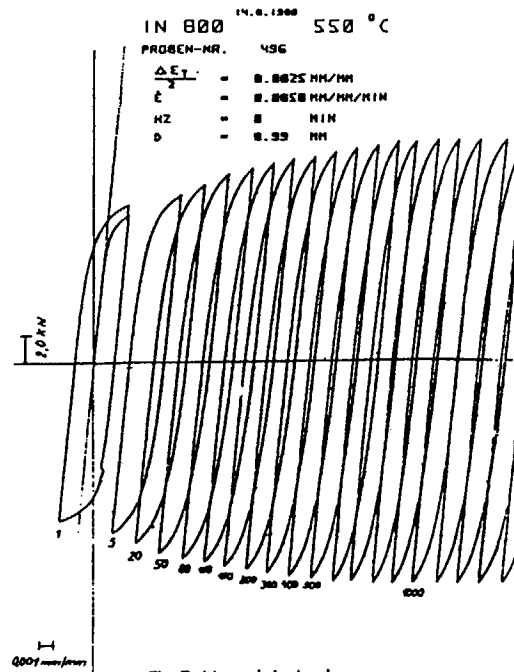


Fig.5 Material test

half a percent strain range at 550 deg C. It can be seen that the material shows a distinct tendency for strain hardening for monotonic and for cyclic loading.

This behaviour has been transferred into stress-strain curves which are useful for inelastic analysis as shown in fig. 6. This figure shows simplified bilinear curves for different temperatures and monotonic and cyclic behaviour. The monotonic curve represents average behaviour at first loading, whereas the cyclic curve is obtained from the tenth cycle of the tests. For reversed loading kinematic hardening is assumed, i. e. a Bauschinger effect is taken into account.

The creep effects have been taken into account for calculating the relaxation of the residual stress field during the hold periods between the transient conditions. A creep equation has been derived from test data and was used in the analyses.

All the other relevant material data are straight forward and have been taken from codes.

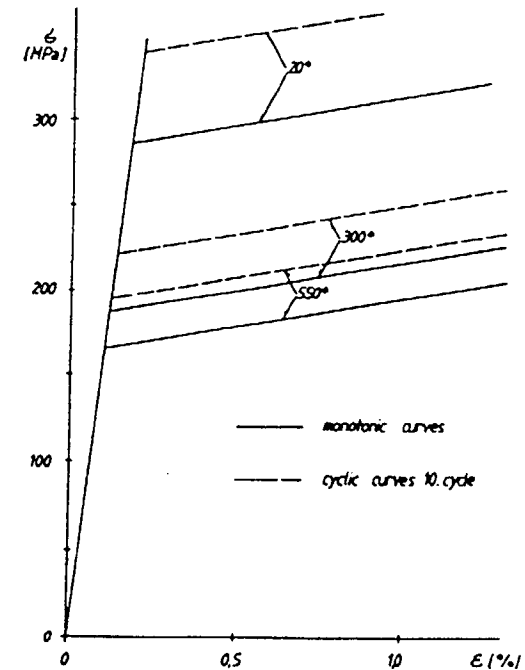


Fig.6 Curves for inelastic analyses

#### 1.4 Thermal analyses

The transient conditions of the three chosen representative ones were analysed with thermal time-history analyses using the finite element mesh of fig. 3. The film coefficients were subject to special consideration and have been generated as a function of time in the nozzle bore and the header bore region. Fig. 7 shows an example of a temperature distribution at a time of 75 sec of the first transient. This transient includes a very rapid shock from 560 deg C down to about 320 deg C, which is the saturation temperature at the lowered pressure during the transient. It can be seen that the nozzle has a much lower average temperature than the thinwalled header which is still predominantly at its original temperature.

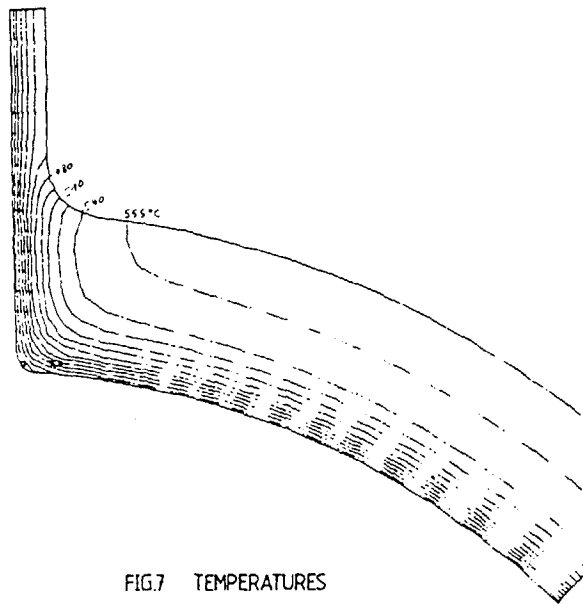


FIG.7 TEMPERATURES

#### 1.5 Structural analyses

The results of the thermal analyses were used to perform the detailed structural analyses with elastic-plastic-creep behaviour. The pressure loading was also applied in the synchronic transient way of the specified operating condition, thus producing the proper ratchetting strains that have to be assessed. The first, most severe transient was analyzed conservatively with the monotonic material data.

whereas the other two were allowed to have hardened yield strength as explained in chapter 3. For each transient two cycles were analyzed in time history procedure. This is necessary because the first cycle starts with no residual stress field and therefore may show considerable shakedown. Fig. 8 shows the strain distribution after two operating cycles of the first transient. The strains are effective plastic strains with a maximum of 0.31 percent at the nozzle bore. It can be seen that the transition between header and nozzle has permanent straining whereas the two undisturbed shell parts have locations with no accumulated strain (dashed line).

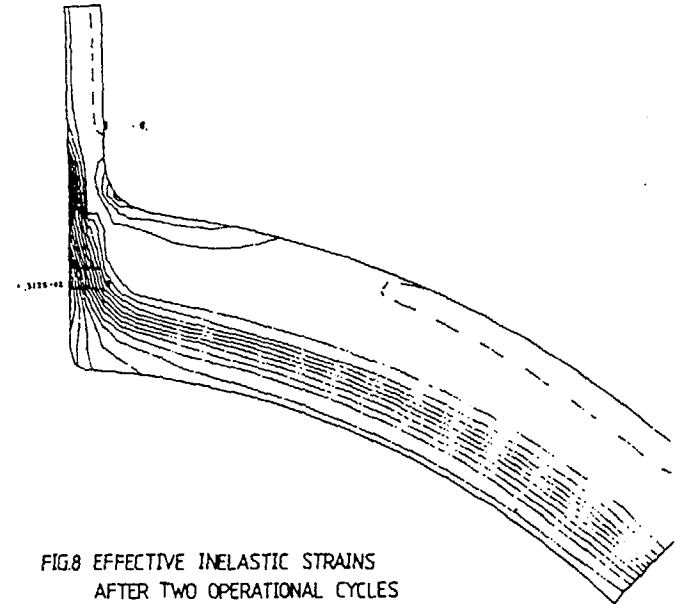


FIG.8 EFFECTIVE INELASTIC STRAINS  
AFTER TWO OPERATIONAL CYCLES

Fig. 9 shows the behaviour of the critical point in the structure in the stress-strain diagram. The first cycle has much more ratchetting strain than the second, but there is not complete shakedown and ratchetting would continue with more cycles.

#### 1.6 Assessment of the results

Since only two cycles have been analyzed for each transient, an extrapolation was performed to assess the final ratchetting strains for all cycles. The limits for these

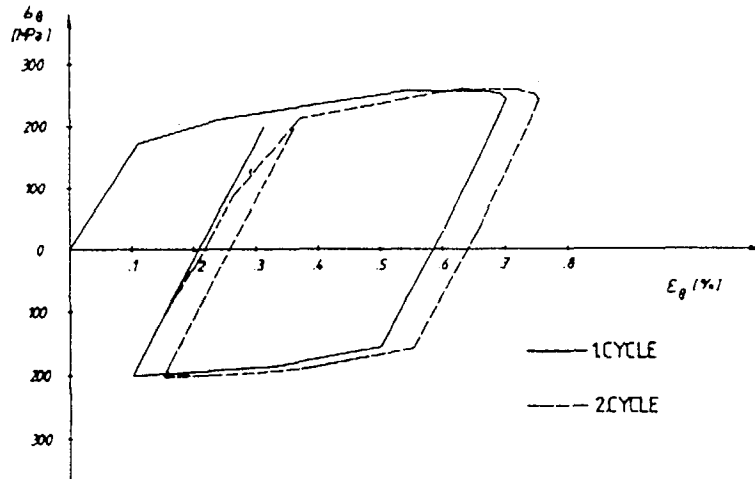


Fig.9 HOOP STRESSES AS FUNCTION  
ON HOOP STRAINS (2 CYCLES)

accumulated strains have been taken from the US elevated temperature code ASME Section III N-47 as 1, 2 and 5 percent strain for average, linearized and peak strain respectively. For the determination of the average and linearized strains, sections across the pressure boundary were considered. The maximum usage of the limits was found to occur in a section at the transition from nozzle to header, with a value of 49 percent.

Besides assessment of the ratchetting strains, the usage by the interaction of fatigue and creep has been assessed. Creep damage was found to be negligible for the material and the temperature and was assessed very conservatively. The fatigue damage part was found to amount to 2.7 percent, which is much less than what was obtained by elastic calculations.

### 1.7 Discussion of the results

The calculations presented have revealed that in contrast to original assumptions the phenomenon of fatigue was not critical. However the phenomenon of ratchetting, i. e. the incremental monotonous accumulation of strain over many cycles, was difficult to bound. Elastic analyses showed that there was no chance of fulfilling the ratchetting limits. The inelastic analyses still revealed a relatively high usage of the limits of almost 50 percent. If one bears in mind that operation can be different from specified transients, the question arises, whether this situation could be improved for a next HTR application.

The first possibility would be operational changes. However it lies in the physical nature of these superheated steam generators that there is quite a difference between the level of saturation temperature and live steam temperature. Relatively minor misbalances of the heat balance during operation, as e. g. overfeeding, causes the endpoint of the evaporation zone to be pushed towards the end of the superheater bundle which results in a drastic drop in temperature at the steam generator end. From fossil fired boilers this phenomenon of overfeeding is also known and cannot always be prevented in upset operating conditions. Experience has shown damages due to such operation in fossil plants.

A better remedy for less susceptibility of such a header probably is a reinforcement of its wall thickness. A heavier wall will slightly increase the calculated fatigue damage, but as shown this is not expected to be critical. The benefit will be in less consumption of allowable ratchetting strain, since this seems to be more critical. Ratchetting is more sensitive to the primary stresses due to internal pressure than to thermal strains. Therefore an optimized increase of the wall thickness would be advisable for the next design to be realized. This does not mean that the THTR headers would not be adequate, it just shows that the wall thickness can still be optimized for maximum safety margin for all failure modes.

## 2. Design for consequences of header rupture

### 2.1 General

The main steam headers are safety related components of the reactor. In case of an unexpected rupture it must be assured that the consequences for other components remain limited. In order to consider a wide spectrum of risks, two typical rupture modes have been assumed at different locations:

- transverse break, with a complete separation of the header in two parts.
- longitudinal break, parallel to the header axis, without separation of the header.

The locations of the breaks can occur at arbitrary points along the headers. The fluid leaving the break exerts large forces onto the header, that have to be taken up by whip restraints. These have the function to restrict the movement of the damaged header in order to protect piping and civil structures in the vicinity.

The calculations of the support loadings during a rupture normally are quite tedious. However in the following it is

shown that these rupture loadings can be determined with sufficient accuracy by using simplified dynamic models.

## 2.2 Concept of the header support

The restraint design must fulfill the function in the normal operating conditions as well as the one due to the large loads imposed by rupture. The chosen design is shown in fig. 10. The support in the ring wall - here called the left support - is designed as a fixation for all six degrees of freedom. The load path is from the header over the thermal sleeve, the flange and the anchor pipe into the concrete wall.

The support at the right end of the header can only take up transverse forces. The header there is free to move in axial direction; of course there may be friction forces. The design gap is sufficient to allow the thermal expansion of the header.

The tie rods between the left support and the ring plate at the right free end of the header take up the axial forces in case of a transverse break. Because the header and the axial tie rods can expand independently, the left end of the tie rods is fixed with disk springs.

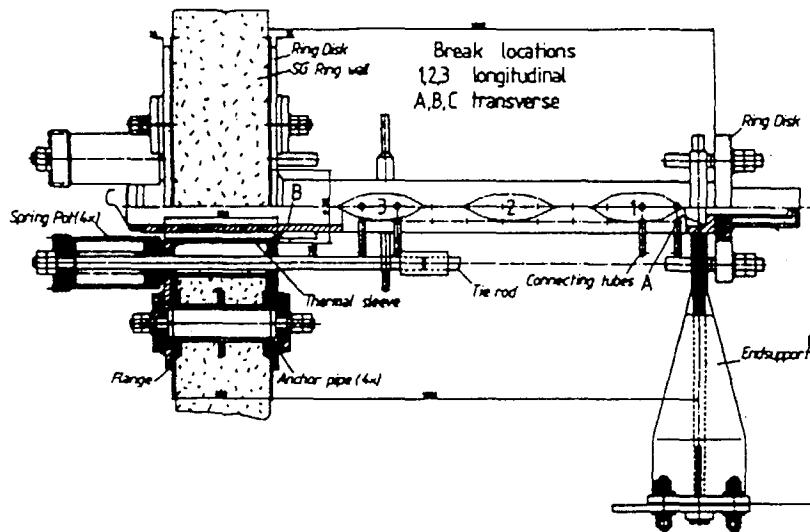


Fig.10 Support Configuration

## 2.3 Support loads at rupture

Fluid dynamic investigations showed that the maximum jet reaction force at transverse rupture amounts to

$$F_0 = 440 \text{ kN}$$

For a longitudinal break the opening section area was assumed twice the pipe i. d. area. The resulting fluid force is in this case:

$$F_0 = 590 \text{ kN}$$

As a function of time the forces can be assumed with sufficient accuracy to rise according to fig. 11 to their full values within 15 msec.

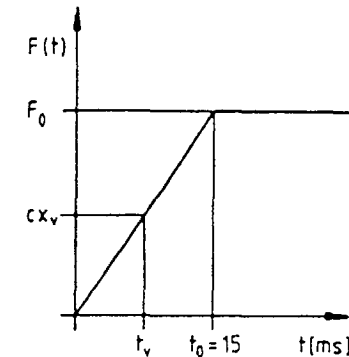


Fig.11 Jet Force Behavior after a Header Break

### 2.3.1 Transverse break

For this type of break it is assumed that it leads to a total separation of the header. The dynamic loads of the two header parts are partly compensated by the tie rods and only the force difference is transmitted through the flange into the ring wall. Because of the large difference in axial stiffness between the flange and the disk springs, the movement of the two separated parts can be treated separately in a model of a dynamic single degree of freedom system each, as shown in fig. 12.

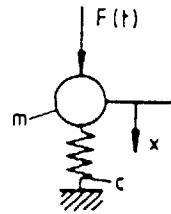


Fig.12 Single Mass Oscillator Model

Without going into details, the equation of motion of a header part can be written for the time greater  $t_0$ :

$$x(t) = \frac{2 F_0}{c w t_0} \sin \frac{w}{2} (t_V - t_0) \cos \frac{w}{2} (2t - t_0 - t_V) + \frac{F_0}{c} \quad (1)$$

with  $w = \text{sqrt}(c/m)$  and  $t_V = \frac{F_V}{F_0} t_0$

$m$  means the mass moved,  $c$  the stiffness of disk springs or flange in axial direction, and  $F_V$  the pretensioning force of the disk springs.

From this the dynamic load factor (DLF) can be determined as the maximum deflection divided by the static deflection under the fluid force  $F_0$ . It amounts to:

$$DLF(l,r) = \frac{2}{w t_0} \left| \sin \frac{w}{2} (t_V - t_0) \right| + 1 \quad (2)$$

The function is shown in fig. 13 depending on the natural frequency  $w$ . The thick line shows the envelope of the values according to:

$$DLF(l,r) = \frac{2}{w t_0} + 1 \quad (3)$$

As mentioned before, the two loadings left (l) and right (r) have to be superimposed for the ring wall. It follows according to fig. 14:

$$DLF = DLF(r) + DLF(l) - 2 \quad (4)$$

The results of the calculations for the rupture locations according to fig. 10 are shown in table 1. The largest and therefore determining loads are therefore resulting from rupture in location C.

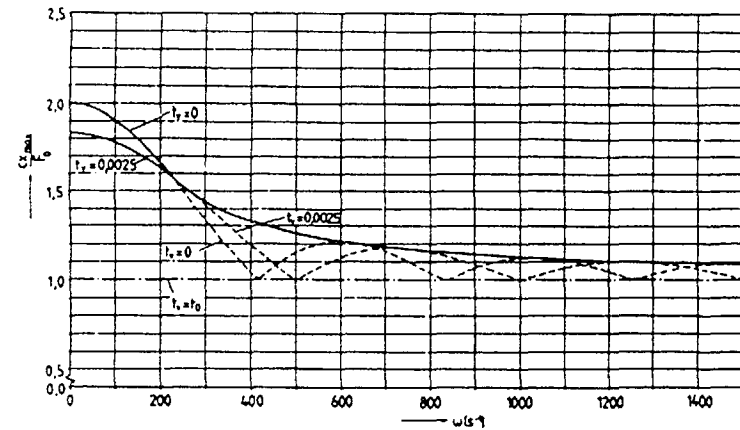


Fig 13 Dynamic Load Factors

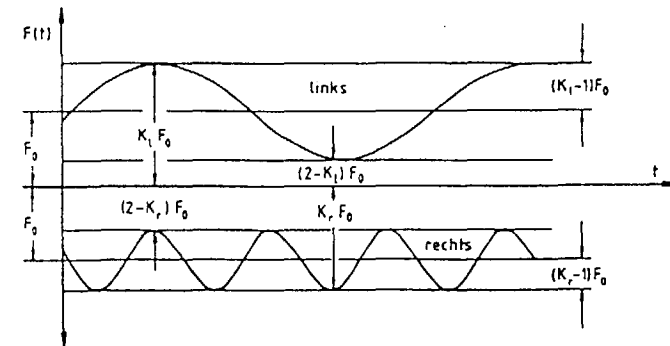


FIG.14 SUPER POSITION OF DYNAMIC LOAD FACTORS

Table 1

jet force $F_0$	kN	440		
break location		A	B	C
natural frequency left	$s^{-1}$	387	472	-
dynamic load factor $DLF_l$		1.35	1.28	-
natural frequency right	$s^{-1}$	132	97	406
dynamic load factor $DLF_r$		1.75	1.78	1.32

### 2.3.2 Longitudinal break

The dynamic calculations for the longitudinal break are much more tedious due to the statically indetermined fixation, the gaps in the supports and the plastification of the header. The calculations are based on a nonlinear beam model with discretized mass points as shown in fig. 15. For the bending properties of the beam it is assumed that the section remains the same. The nonlinear material response is approximated by a bilinear stress-strain relationship. The calculations were performed with a computer program on the basis of transfer matrices. The rupture locations are assumed at three relevant points along the header axis. Fig. 16 shows the loadings of the header right end support, whereas figs. 17 and 18 show the loading on the left fixation. Finally, fig. 19 shows the maximum bending moments in the header itself. The full line curves are for rupture location 1, the dashed lines for 2 and the dash-dot lines for 3.

It is shown that the support loadings are well acceptable despite the gap of 3 mm between header and support.

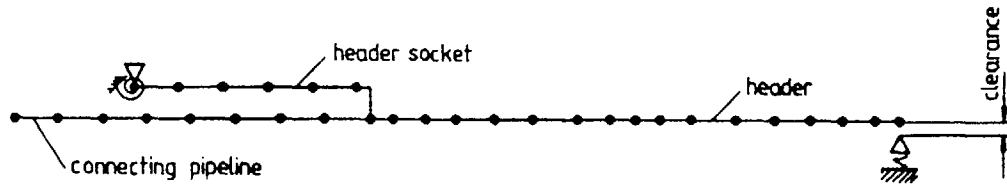


Fig 15 Multiple Mass Oscillator Model

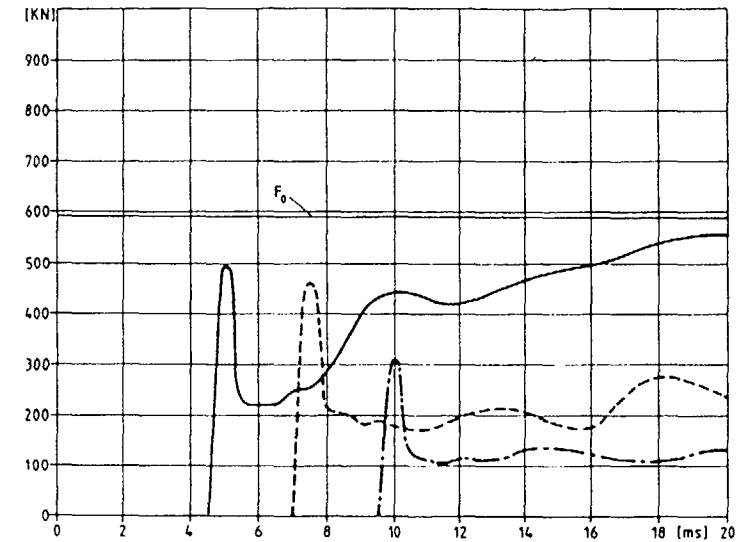


Fig.16 Loadings on header right end support for longitudinal break

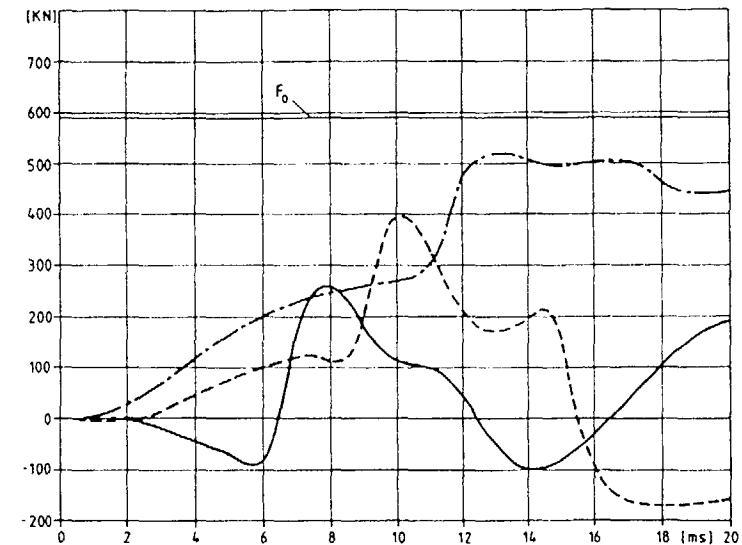


Fig.17 Force Loading on support flange for longitudinal break

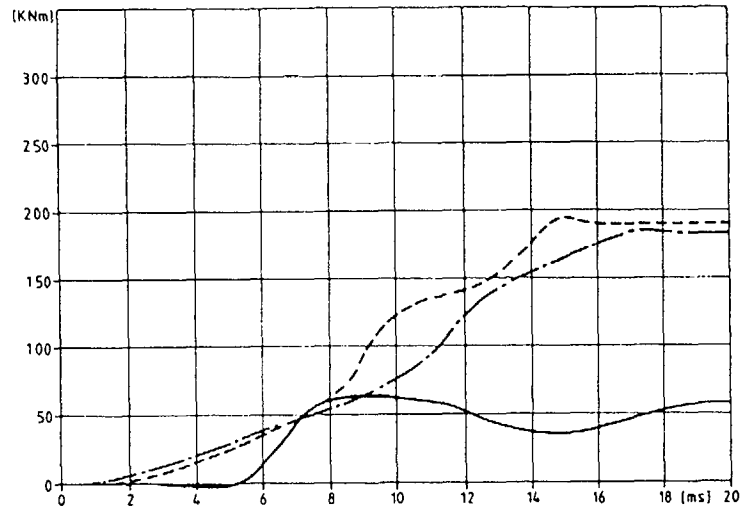


Fig.18 Moment Loading on support flange for longitudinal break

### 3. Conclusions

The high pressure headers of the THTR steam generators have been analysed extensively to show, that a header rupture should not occur because of service loadings. It also has been shown that in the event of an unexpected rupture the consequences can be limited to the header itself by the installation of heavy whip restraints.

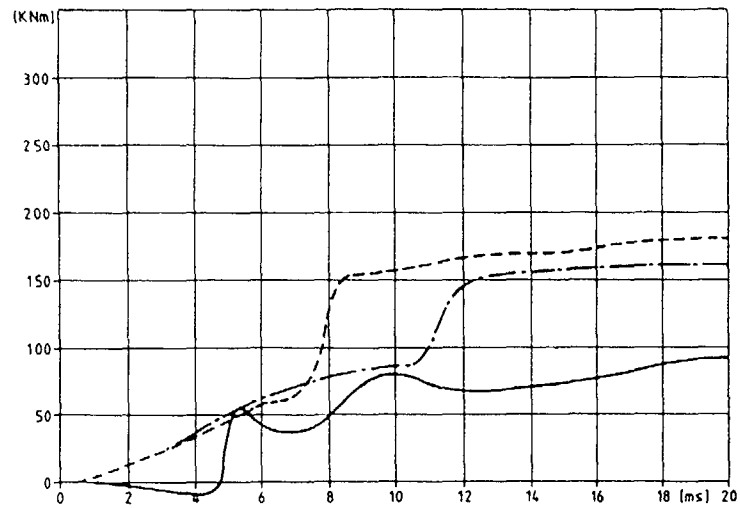


Fig.19 Maximum moments across header section